SmartPark as a Virtual STATCOM

Pinaki Mitra, *Member, IEEE*, Ganesh Kumar Venayagamoorthy, *Senior Member, IEEE*, and Keith A. Corzine, *Senior Member, IEEE*

***Abstract*—Power electronic-based FACTS devices such as STATCOMs are sometimes essential for voltage support in transmission networks. They can also be used for continuous operation of doubly-fed induction generator-based wind turbines during faults. However, these devices are quite expensive and therefore cannot be used extensively. This paper explores the potential of a low-cost solution that utilizes the reactive power and voltage support capabilities of plug-in vehicles parked in charging stations (SmartParks) so that they can behave as virtual STATCOMs. For this solution, a 12-bus multimachine power system is considered wherein one of the conventional units is replaced by a 400 MW wind farm. Twelve SmartParks are developed and integrated into the test system. First, they are connected to a weak bus in the system and used in voltage control mode. Their performance is compared with a STATCOM of a similar rating. Next, the SmartParks are connected to the wind farm bus, and a coordinated reactive power control strategy is proposed to improve the fault-ride-through capability of the wind farm without exceeding the current limits of rotor and grid-side converters. The entire study is carried out in real time on a real-time digital simulator platform.**

***Index Terms*—Doubly-fed induction generator, plug-in vehicles, real-time digital simulator, SmartParks, STATCOM.**

I. Introduction

THE NUMBER OF plug-in electric vehicles (PEVs) entering the market has been increasing very rapidly in recent years. In the near future, these vehicles could participate in vehicle-to-grid (V2G) power transactions in the proposed smart grid framework. Since most personal vehicles in the US are parked more than 95% of the day and generally follow a daily schedule [1], their predictable nature can be utilized successfully in V2G transactions. During V2G operations, the PEV fleet can provide many grid services, such as regulation and spinning reserve [1], [2], load leveling [3], serving as external storage for renewable sources [4], and generating revenue by buying and selling power at different times according to variable price curves [5], [6]. Another important service that these PEVs are capable of is reactive power support, which has not been studied extensively. The reactive power compensation capability of an individual vehicle battery has been reported in [7], where the common dc bus of the dc-dc converter and the inverter are responsible for reactive power compensation. The dc-dc converter charges the battery using the constant-current-constant-voltage algorithm. In the approach presented in [8], the dc-dc converter is not used; instead, the battery is connected directly to the inverter. The reactive power capability of a single vehicle has been utilized in a residential-level power system. These previous studies have not dealt with the reactive power capabilities of a fleet of such vehicles parked in a charging station (SmartPark) or their usefulness, in bulk amounts, in a transmission network. This paper presents a methodical way to analyze the active and reactive power transaction capabilities of a realistic vehicle battery in the V2G mode of operation. Based on the capabilities of an individual vehicle, a SmartPark model consisting of a fleet of such vehicles has been developed and integrated into a 12-bus power system.

Shunt Flexible AC Transmission System (FACTS) devices such as static compensators (STATCOMs) are capable of very fast and accurate reactive power compensation [9]. However, the main drawback of FACTS devices is their high cost. On the other hand, the PEVs, while parked in the SmartParks, contain a significant amount of active and reactive power potential and can be utilized for meeting the grid's requirements with little significant infrastructure cost. Most importantly, the added advantage of reactive power is that it can be injected to the grid without lowering the battery's state of charge (SOC). A very small amount of real power will be lost during this reactive power transaction process, so the vehicles' batteries will have to supplement the difference. However, for such a small amount of real power loss, the net reduction in the state of charge of the individual batteries will be negligible. Therefore, only a centralized controller will be needed at the SmartParks to make this idea a reality. With that control, it is possible for these SmartParks to behave like virtual STATCOMs. The idea of utilizing a photovoltaic solar farm as a STATCOM at night has been referred to in [10]. A similar service could be obtained from SmartParks in future smart grid infrastructures.

STATCOMs can also be used for uninterrupted operation of the doubly-fed induction generator (DFIG) based wind farms in grid-connected mode during grid faults [11], [12]. It is a common practice for DFIG-based wind turbines to block the rotor side converter (RSC) during the fault and to short-circuit the rotor terminals with a crowbar [13]. During that period, the wind turbine generator behaves as a squirrel cage induction generator and absorbs reactive power. One way to supply this reactive power is to set the grid-side converter (GSC) to reactive power and voltage control mode during that period. However, if the network is weak, the reactive power supplied by the GSC may not be sufficient. Hence, additional reactive power support from STATCOM-like devices is necessary. In [11], a STATCOM was used in voltage control mode to serve this purpose, but no coordination existed between the control

Manuscript received August 07, 2010; revised February 27, 2011; accepted May 01, 2011. Date of publication July 14, 2011; date of current version August 24, 2011. This work was supported by the National Science Foundation, under Grant EFRI #0836017. Paper no. TSG-00105-2010.

P. Mitra is with ABB, 600089 Chennai, India.

G. K. Venayagamoorthy and K. A. Corzine are with the Real-Time Power and Intelligent Systems Laboratory, Missouri University of Science and Technology, Rolla, MO 65409 USA (e-mail: gkumar@ieee.org).

Color versions of one or more of the figures in this paper are available online at http://ieeexplore.ieee.org.

Digital Object Identifier 10.1109/TSG.2011.2158330

of the STATCOM and the GSC; hence, during the postfault period, when the STATCOM injects a significant amount of reactive power, the GSC absorbs such a major portion of it that it almost exceeds its limits. An intelligent coordinated reactive power control strategy between the GSC of a large wind farm and a STATCOM was proposed in [12].

The ideas presented in [11] and [12] for fault-ride improvements through a wind farm have been extended in this paper, and a different coordinated control strategy has been proposed. In this paper, instead of a STATCOM, similar performance has been achieved from SmartParks when they are used as virtual STATCOMs in coordination with the GSC of a 400 MW wind farm in a 12-bus system.

In the studies presented in this paper, modeling of the entire system along with the vehicle battery and inverter, the DFIG and all the controls are carried out on a real-time digital simulator (RTDS) platform. The advantage of using RTDS is that, it represents the detailed dynamics of an actual power system. Even the fast acting power electronic switching devices can be simulated in the RTDS in such a way that it can be interfaced with a practical hardware system any time. The simulation of switching devices runs in smaller time steps on giga processor RTDS cards—the GPC cards. GPC is a powerful computational unit which can be used for solving the overall network solution as well as auxiliary components. A GPC contains two IBM PowerPC 750GX RISC processors each operating at 1 GHz. In addition to the network solution and the simulation of standard power system components at 50 μs time step, the GPC card provides small time step ($< 2\,\mu$s) simulations for voltage source converters (VSC). This increase in accuracy allows for better representation of switching components in a real-time environment. Another important issue is the simulation time. If such a detailed nonlinear representation of the switching devices are to be accommodated in a non-real-time simulation platform such as PSCAD or MATLAB, and the simulation time-step is maintained at a sufficiently lower value than the switching time-step, then the dynamic simulation takes a very long time. A few seconds' simulation can sometimes take a few hours. Whereas, on the RTDS platform, a second simulation takes exactly a second without comprising any detail in the representation of switching devices.

II. Development of a SmartPark Model

In order to develop a SmartPark model and to utilize it as a virtual STATCOM, it is essential to realistically assess the $P-Q$ capability of an individual PEV. To obtain that capability curve, the PEV is represented by a dc voltage source, followed by a bidirectional three-phase inverter, as shown in Fig. 1. The dc source is considered ideal. The value of series resistance is 0.005 ohm. The inverter generates a 208 V three-phase line-to-line rms voltage, which then passes through a transformer to connect to the utility. Between the inverter and the transformer, there is a small inductance.

The control strategy for the vehicle inverters is presented in Fig. 2. The active and reactive powers at the output of the inverter in the $d-q$ reference frame are expressed as [14]

$$P = \frac{3}{2}(v_{qs}i_{qs} + v_{ds}i_{ds}) \tag{1}$$

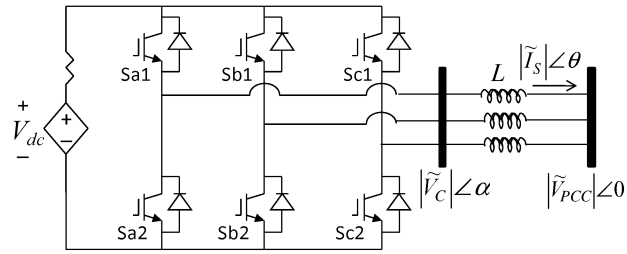

Fig. 1. PEV representation by dc voltage source (battery) followed by an inverter.

$$Q = \frac{3}{2}(v_{qs}i_{ds} + v_{ds}i_{qs}). \tag{2}$$

In a synchronously rotating reference frame, the peak line-to-neutral voltage lies on the q-axis, and $v_{ds} = 0$. Therefore, the objective of the control is to command the currents corresponding to the demanded power, as follows:

$$i_{qs}^* = \frac{2}{3}\left(\frac{P^*}{v_{\text{peak}}}\right) + \frac{K_i}{s}(P^* - P) \tag{3}$$

$$i_{ds}^* = \frac{2}{3}\left(\frac{Q^*}{v_{\text{peak}}}\right) + \frac{K_i}{s}(Q^* - Q). \tag{4}$$

The first component on the right-hand side of (3), (4) is based on the power equations (1), (2), where v_{peak} is the filtered line-to-neutral peak voltage. The filter time constant is 20 ms. This component creates fast responses to sudden changes in commanded power. The integral term eliminates steady-state error. Therefore, the control action is essentially a summation of an integral control and a nonlinear feedforward path. The q- and d-axis commanded currents are then transformed into an $a-b-c$ reference frame, and the switching pulses are generated by delta current-regulation.

As shown in Fig. 2, a limit is placed on the commanded current to prevent a large current from flowing through the vehicle battery and inverter during adverse grid interactions. However, if the i_{qs}^* or i_{ds}^* hits the upper limit and the error is still positive, the error accumulates through the integrator. Then, when the control action is supposed to reduce, this accumulated error prevents it from coming down to the desired value. This creates an overshoot and delays settling. Similar events occur when the control action hits the lower limit and the error is still negative. In order to solve this problem, an anti-windup strategy is used. This strategy resets the integrators in the two situations mentioned above. A number of more efficient and elaborate anti-windup strategies exist. This particular strategy is used in this paper because of its simplicity, and it served its purpose quite nicely. However, resetting an integrator creates a discontinuity in the system that could result in additional complexities in the system's dynamics. A thorough investigation of different anti-windup strategies is beyond the scope of this paper, but a detailed analysis of anti-windup strategies can be found in [15].

With this control, the $P-Q$ capability of a realistic vehicle battery is now studied. Since battery capacity and specific energy increase every year, and the V2G transaction is a futuristic scenario, it is better to study the $P-Q$ capability of a realistic

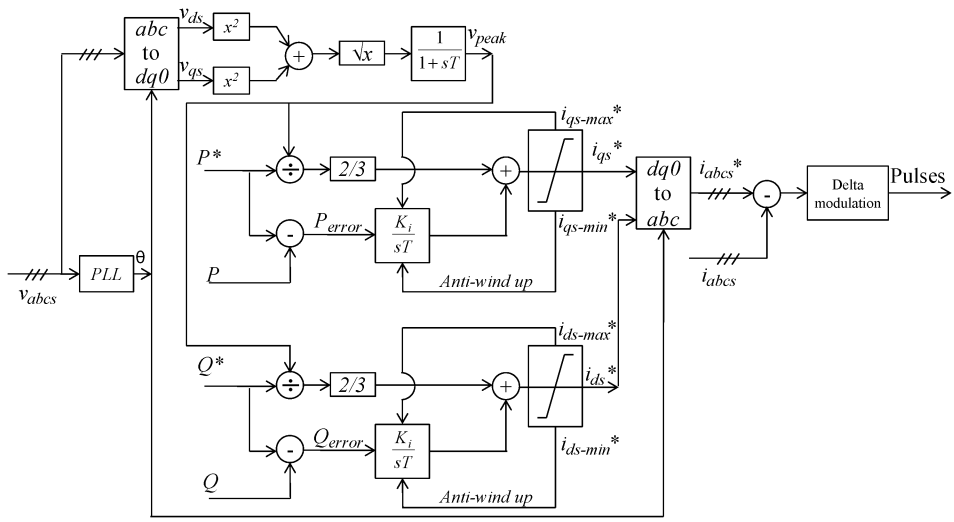

Fig. 2. The proposed current control strategy [14].

TABLE I
RELEVANT BATTERY SPECIFICATIONS (HEMV-7) [16]

Nominal voltage at 50% SOC	307 V
Charge limit	344 V
Discharge limit	210 V
Maximum continuous current at 25^0 C	200+ A
Peak power at 50% SOC	138 kW
Continuous power at 50% SOC	74 kW
Energy	9.2 kWh
Capacity	30 Ah

battery with high power and high specific energy. An Li-ion battery system used for hybrid electric military vehicles (HEMV-7) [16] is therefore considered for this study. Its nominal voltage at 50% SOC is 307 V. The Li-ion battery system referred to in [16] is obtained by packaging 5 to 8 modules of 12 cells of VL 34 P Li-ion cells. The relevant specifications of that battery system are presented in Table I.

The $P-Q$ capability of such a battery is obtained as follows:

The phasor diagram corresponding to the system in Fig. 1 is shown in Fig. 3. Two factors are considered for sizing the line inductance L. A higher inductance value reduces the THD of $\widetilde{I}_S$ but at the same time limits the active and reactive power capability at a particular battery voltage. Since the battery is assumed to be connected to the utility grid through the inverter, there should be strict THD requirements on the grid side. A less than 5% THD requirement is considered in this paper. At a rated continuous power (74 kW) from the battery, the THD of the current ($\widetilde{I}_S$ in Fig. 1) waveform is analyzed for different values of L. It is observed that a minimum value of $L = 0.08$ mH gives a THD of 4.97%, which is chosen in this paper. The ratings of inverter components depend on the limiting value of $|\widetilde{I}_S|$, and can be determined considering that the battery is supplying the rated peak power (138 kW) in a steady state at unity power factor. Considering $|\widetilde{V}_{\mathrm{PCC}}| = 208$ V, $|\widetilde{I}_S|$ can be obtained from the following equation:

$$3 \cdot |\widetilde{V}_{\mathrm{PCC}\_ph}| \cdot |\widetilde{I}_S| = S = \sqrt{P^2 + Q^2} \tag{5}$$

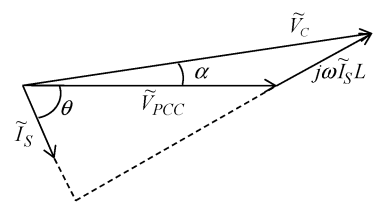

Fig. 3. Phasor diagram corresponding to Fig. 1.

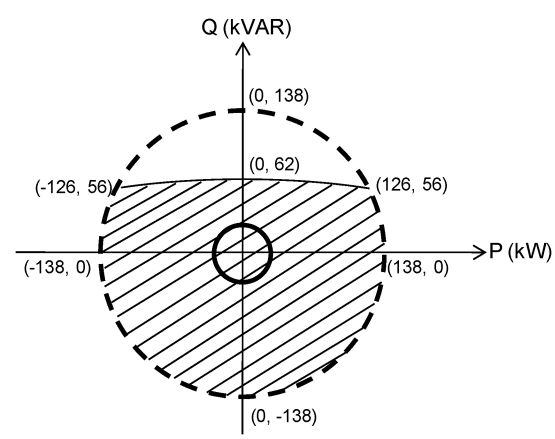

Fig. 4. Ideal and actual $P-Q$ capability curves of the 307 V and 9.2 kWh battery.

In (5), $|\widetilde{V}_{\mathrm{PCC}\_ph}|$ is the magnitude of the rms phase voltage, and S is the total apparent power. The ideal $P-Q$ capability curve is now obtained from (5), with the maximum $|\widetilde{I}_S|$ value being used as a constraint. This curve, a perfect circle, is represented by the dotted line in Fig. 4. For the given battery, P and Q vary within ± 138 kW and ± 138 kVAR, respectively.

When the battery delivers a high reactive power, the angle α (Fig. 3) decreases; consequently, $|\widetilde{V}_C|$ increases compared to $|\widetilde{V}_{\mathrm{PCC}}|$. The minimum dc voltage required to produce $|\widetilde{V}_C|$ is given by

$$V_{dc\_\min} = \sqrt{6} \cdot |\widetilde{V}_C|. \tag{6}$$

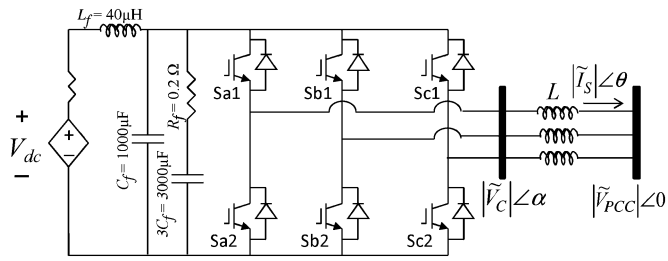

Fig. 5. Battery with filter.

Using this additional constraint, the actual $P-Q$ capability curve at 50% SOC is obtained which is shown by the shaded region of Fig. 4.

One important issue, the current-carrying capacity of the connector at home or at the SmartParks, will affect the actual $P-Q$ capability in practice. Currently, connectors are manufactured for one-way charging with a much lower rating than the peak power rating of a standard vehicle battery. For example, according to the SAE J1772 update, ac level 2 charging is capable of carrying 19 kW of power and a current of up to 80 A [17]. A charging facility with higher ratings, such as ac level 3 charging with a power rating in the range of 60–150 kW, is also available [18]. It is quite reasonable to expect new high-capacity two-way connectors in the future, when V2G transactions will actually take place. However, in order to represent a realistic scenario, in this paper, the continuous current carrying capacity of the charging facility is considered to be 70 A, which restricts the continuous active and reactive power capability of the vehicle within the range of ±25.2 kW and ±25.2 kVAR, respectively. Here, the "+" sign means the vehicle is selling power to the grid, i.e., it is in discharging mode, and the "−" sign indicates that it is buying power from the grid, i.e., it is in charging mode. This is denoted by a solid circular line inside the shaded region in Fig. 4.

Importantly, when reactive power is commanded from the battery, the battery current contains high-frequency harmonic components. In order to eliminate these high-frequency components, a filter is designed with a cut-off frequency (ω_c) of 800 Hz. The filter is shown in Fig. 5, where L_f, C_f and R_f are related by the following (7), (8):

$$\omega_c = \frac{1}{\sqrt{L_f C_f}} \tag{7}$$

$$R_f = \sqrt{\frac{L_f}{C_f}}. \tag{8}$$

Based on the active and reactive power capabilities of an individual vehicle obtained above, SmartPark models are developed. The same battery-inverter model (Fig. 1) now represents a SmartPark consisting of hundreds of such vehicles. The SmartPark is connected to the respective SmartPark bus through a 208 V/22.0 kV step-up transformer. The ratings of the inverter and the control parameters are modified accordingly. The controls of these SmartParks (inverters) are designed such that they are capable of ±25 MW of power transaction with the grid. Considering that the average power transaction capabilities of individual vehicles is ±25.2 kW, each of these parking lots should contain nearly 1000 vehicles to achieve that capability. In a typical city, it is quite reasonable to assume that there will be several large parking lots (at shopping malls, airports, etc.) distributed throughout the city in distances of one to a few kilometers with similar or even greater vehicle capacity. The reactive power capabilities are also designed as ±25.2 kVAR from each vehicle and thus are a total of ±25 MVAR from each parking lot.

When the SmartParks are used in voltage control mode, an additional voltage control loop is used in the control strategy, which is otherwise similar to that of an individual vehicle inverter. In voltage control mode, the bus rms voltage is first compared with the reference voltage, and the error is passed through a PI controller to generate the reactive power command for the SmartParks. This control strategy is presented in Fig. 6.

III. Modeling the Test System

A. Modeling the Overall System

The test system considered in this paper is a standard 12-bus power system originally proposed in [19] to evaluate the effects of FACTS devices in the transmission level. The system has four generators and three interconnected areas. Generator G1 represents the infinite bus (Fig. 7). In this study, a 400 MW wind farm replaces generator G4.

In order to have a significant reactive power compensation capability that matches the system's requirements during voltage control, 12 SmartParks (PL1 to PL12) with equal ratings, as mentioned in the previous section, are integrated to the system. Previous studies have shown that in the 12-bus system, bus 4 in Area-3 has the lowest voltage under normal conditions [20]. Therefore, in the first case study, SmartParks are indirectly connected to bus 4 in order to compare their voltage control capability with that of a STATCOM. The SmartParks are connected directly to bus 13 (Fig. 7), an additional bus added to the original 12-bus system in order to connect the SmartParks. Bus 13 is connected to bus 4 through 22.9 kV/230 kV step-up transformers.

In the second case study, when the SmartParks are used to improve the fault-ride-through capability of the wind farm, all 12 SmartParks are indirectly connected to bus 6 where the wind farm is connected, as shown in Fig. 8.

B. Modeling the Wind Farm

The wind farm is equipped with a Doubly Fed Induction Generator. It uses back-to-back PWM converters for variable speed wind power generation. The control objective of the grid-side converter is to keep the dc link voltage constant regardless of the magnitude and direction of the rotor power. A stator-oriented vector control approach is used where the direct axis current controls the dc link voltage and the quadrature axis current controls the reactive power, and, in turn, the voltage at the point of common coupling.

The above mentioned control strategy is similar to that discussed in the research literature [21]. The only difference is that an additional PI controller is used to generate the reactive power command for the grid-side converter from the voltage error signal. The objective of the rotor-side converter is to control the active and reactive power from the stator. This is achieved by

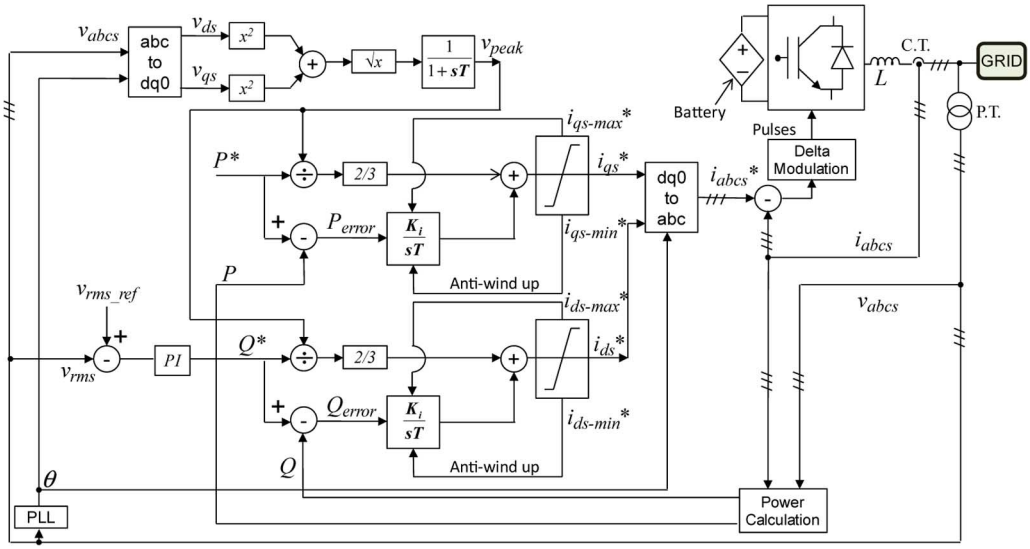

Fig. 6. The proposed control strategy in voltage control mode.

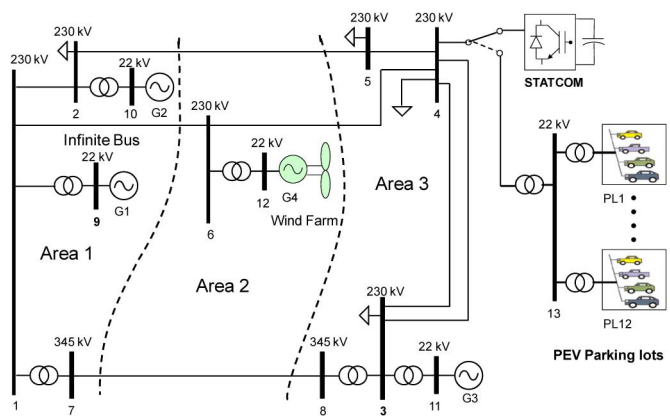

Fig. 7. Case study 1: The 12-bus system with 12 SmartParks indirectly connected to bus 4.

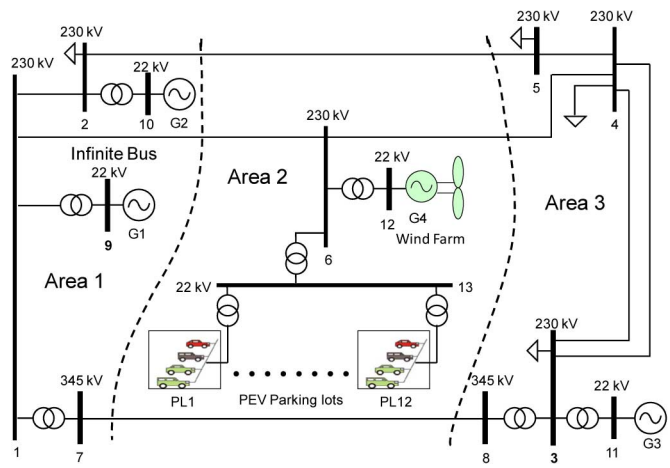

Fig. 8. Case Study 2: The 12-bus system with 12 SmartParks indirectly connected to bus 6.

putting the d-axis of the rotor reference frame along the stator flux vector. The q-axis current reference is generated directly from the commanded electrical power, and the d-axis current reference is generated from the commanded stator reactive power. The electrical power command is generated from the optimum operating point-tracking strategy discussed in [21], when the wind speed is below a certain value. The pitch control does not work at that time, and the wind turbine captures the maximum possible energy at that wind speed. However, if the wind speed exceeds a certain value, the pitch control limits the power generated by the wind turbine. The relevant mathematical equations for the rotor-side and grid-side converter controls are mostly similar to [21] and hence are not described in this paper. The data for the 400 MW wind farm is taken from [12]. All the symbols used in Fig. 9, which presents the schematic diagram of the control strategy, carry their usual meanings and are explained in [12]. The compensation terms for the rotor-side converter in Fig. 9 (v_{dr2} and v_{qr2}) are expressed as follows:

$$v_{dr2} = -s\omega_s \sigma L_r i_{qr} \tag{9}$$

$$v_{qr2} = s\omega_s \left(\sigma L_r i_{dr} + L_m^2 i_{ms}/L_s\right) \tag{10}$$

where

$$\sigma = 1 - L_m^2/L_s L_r. \tag{11}$$

C. Modeling the STATCOM

In order to compare the performance of the STATCOM with 12 SmartParks of ±25 MVAR capacity, a 300 MVAR STATCOM is considered. The switch in Fig. 7 can toggle between the two positions to connect either the STATCOM or the SmartPark bus (bus 13) to bus 4. The STATCOM is used in voltage control mode with a control strategy similar to [11], as shown in Fig. 10. One PI controller generates the d-axis current reference while maintaining the dc-bus voltage of the STATCOM at a constant value, and the other PI controller generates the q-axis current reference with an objective to maintain the voltage at bus 4 at a desired level. The other two PI controllers keep track of the reference currents, and their outputs are added to the cross coupling compensation terms to produce d and q-axis commanded voltages. Those voltages are converted to an $a-b-c$ reference frame, and the pulses are generated by sine-triangle modulation.

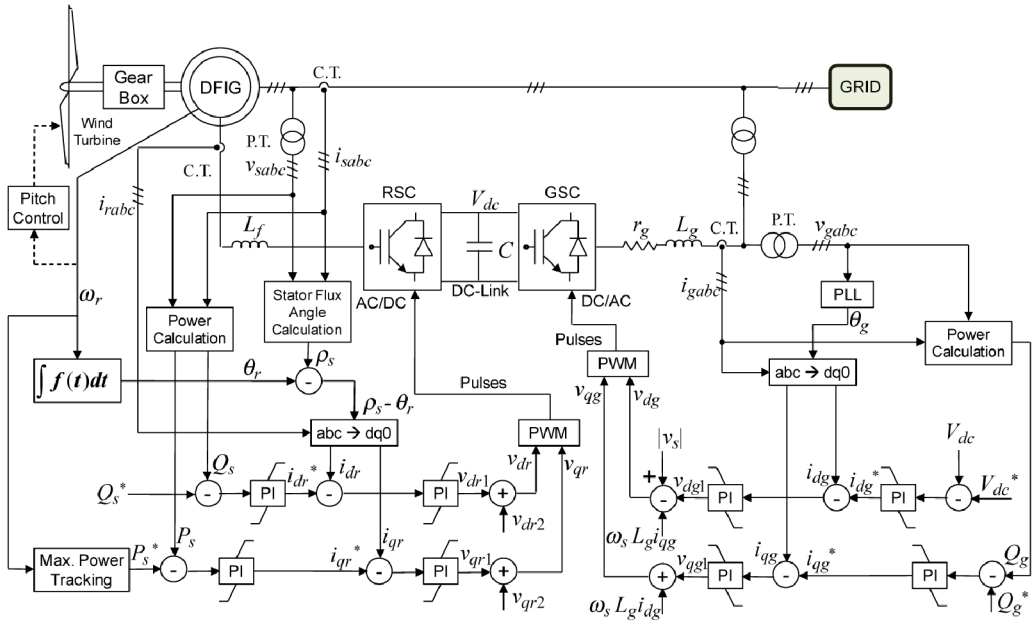

Fig. 9. Control of the wind farm.

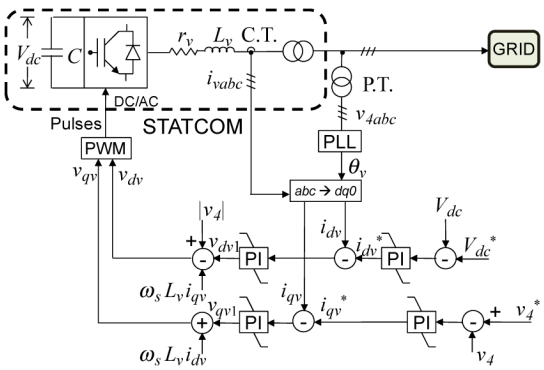

Fig. 10. Control of the STATCOM.

The entire system's PI controllers are tuned by trial and error following the common industry procedure for large-scale, nonlinear systems, as mentioned in [24].

IV. Coordinated Reactive Power Control Strategy

It is well known that during a fault and the consequent stator voltage sag, a dc component is produced in the stator flux [22] which induces large voltage in the rotor circuit; consequently, the rotor current increases to a very high value. Since the RSC is rated at only 30% of the wind farm rating, it is necessary to protect it from the over-current during the transient. Generally, in those situations, a common practice is to use the crowbar protection scheme [23]. However, in the case of a severe fault very close to the wind generator, when the RSC is blocked and crowbar protection is active, the transient changes in the dc-link voltage will command sudden changes in the d-axis current reference and the PI controller, which tracks the d-axis current reference as it reaches its limit. Also, for the sake of continuous operation and reactive power support during this crowbar protection period, sometimes GSC is used in voltage control mode. However, the sudden drop in stator voltage will command large q-axis current from the GSC, which will saturate the other PI controller (which tracks the q-axis current). When both of these PI controllers go into saturation, the d and q-axis commanded voltages are no longer accurate, and the GSC loses control. Effectively, it starts behaving like an open loop system, and the windup problem occurs. Therefore, in this case also, anti-windup strategies should be adopted to prevent the windup problem. During this period, the GSC current might also increase to a very high value, thus inadmissibly damaging the converter. This might even cause the wind farm to trip, and the operation would no longer remain continuous.

In the test system previously described (Fig. 8), this situation is observed (without the SmartParks) when a three-phase-to-ground, 10-cycle fault is applied on bus 6, where the wind farm is connected. During the fault, when the RSC is blocked, the crowbar protection is active, and the GSC is in voltage control mode, the reactive power injection from the GSC rises above 1.0 p.u. although it is designed only for 0.3 p.u. The current in the GSC reaches 30 kA when the rated peak rms current is only 16 kA, as shown in Fig. 11. In order to avoid such a situation, i.e., to prevent the GSC current from reaching such a high value, it can also be blocked at the same time with the RSC. However, in that case, the DFIG will fail to supply the necessary reactive power to which it is sometimes committed per the requirements of some utilities. In this situation, the need for external reactive power compensation is essential and can be served either by a STATCOM or by the SmartParks used as virtual STATCOMs, as proposed in this paper.

SmartParks should be coordinated with the GSC as follows: when crowbar protection is active and both the RSC and GSC are blocked, the SmartParks should be switched to voltage control mode. As soon as crowbar protection is deactivated (after a small time delay of five cycles from the instant of fault clearance) and the RSC and GSC restart switching, the task of voltage control should be switched from the SmartParks to the GSC. In

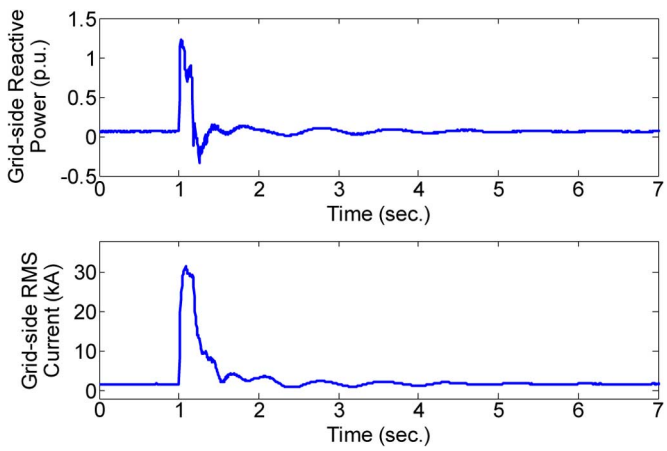

Fig. 11. Performance of GSC during a severe fault while crowbar protection is active and the RSC is blocked.

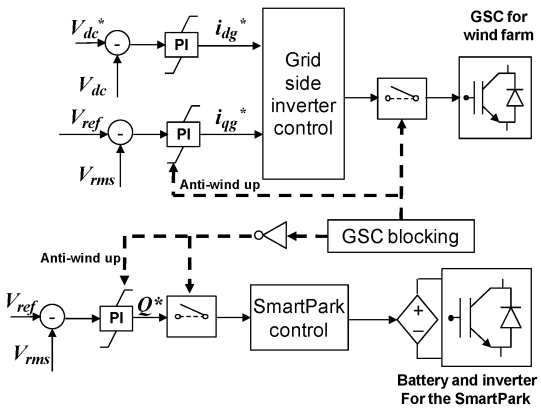

Fig. 12. The coordinated reactive power control strategy.

the presence of external reactive compensation, it is not necessary for the GSC to restart switching simultaneously with the RSC. It can be delayed for a short period of time. Realistically, SmartParks can satisfy the very limited duration for which this external reactive power compensation is demanded for this strategy. The schematic diagram for this coordinated control is shown in Fig. 12. The two integrators, one which generates the q-axis current command for the GSC and the other which generates the reactive power command for the SmartParks from the bus voltage deviation, should be reset while the respective controllers are not active to prevent integrator windup, as shown in Fig. 12.

It is important to mention that the first changeover of the control mode from GSC to SmartPark occurs when a fault exists, and, consequently, the GSC is blocked. During the fault period, the voltage of the wind farm bus is determined primarily by the nature and intensity of the fault, which could force the bus voltage to almost zero. Therefore, the changeover of the control mode during the fault period does not have any visible impact. Similarly, as mentioned above, the GSC restarts switching after a time delay from the instant of fault clearance. Within that delay period, due to the action of the SmartParks in voltage control mode, the voltage of the wind farm bus restores to a value that is very close to 1.0 p.u. The commanded voltage for the GSC in voltage control mode is also 1.0 p.u. Therefore, the second changeover in control mode occurs when the actual

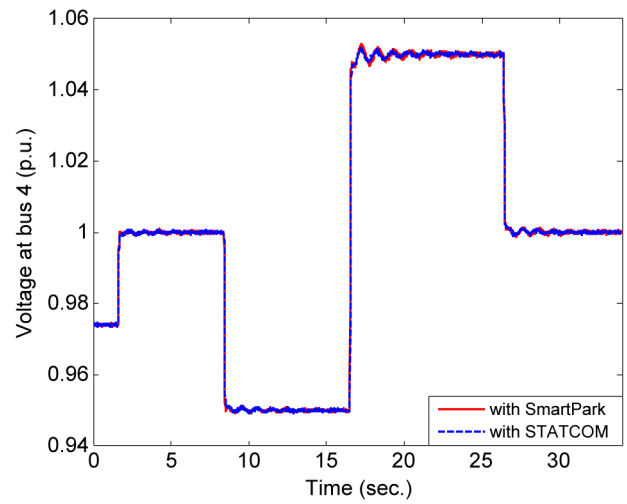

Fig. 13. Comparison of performance between the STATCOM and SmartParks during voltage regulation at bus 4.

voltage of the bus is almost equal to the commanded voltage and the voltage error input to the PI controller is almost zero. Therefore, the changeover in control mode remains fairly smooth, and no bumps are observed.

V. Real-Time Simulation Results

In regards to SmartParks, two different case studies are presented. In the first case study, the performance of the SmartParks in voltage control mode is compared with a STATCOM when it is connected to bus 4 (Fig. 7). In the second case study, the reactive power support from the SmartParks is coordinated with the GSC of the wind farm at bus 6 (Fig. 8), and the performance improvement is presented.

A. Case Study 1

Without any reactive power compensation, the nominal voltage at bus 4 is 0.974 p.u. In order to establish that the SmartParks can behave like a virtual STATCOM, the voltage at bus 4 is commanded from its nominal value to 1.0 p.u. From 1.0 p.u., it is then commanded to 0.95 p.u., from 0.95 p.u. to 1.05 p.u., and then finally back to 1.0 p.u. A similar experiment was carried out with a 300 MVAR STATCOM, and these two performances are compared. Fig. 13 shows that SmartParks behave exactly like the actual STATCOM for the entire range of the permissible bus 4 voltage. Fig. 14 compares the reactive power injection from the STATCOM and from the 12 SmartParks. The same amount of reactive power was injected or absorbed during the voltage regulation study.

Next, an experiment was carried out to study the impact of wind speed variation on the system and to observe how the SmartParks respond to the situation. Initially, it is assumed that the wind speed is 10 m/s; at that speed, the wind farm generates 190 MW. At this point, the voltage at bus 4 is 0.974 p.u. without any reactive compensation. With the SmartParks in voltage control mode, that voltage can easily be regulated to 1.0 p.u. as before. Now, suddenly, the wind speed changes from 10 m/s to 12 m/s, which changes the wind power generation to 350 MW. Without any voltage regulation, this change in wind power moves the entire system to a new operating point where the

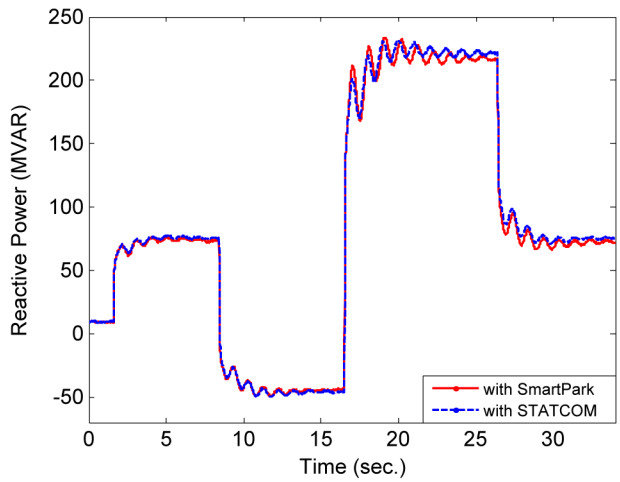

Fig. 14. Comparison of reactive power injection between the STATCOM and SmartParks during voltage regulation at bus 4.

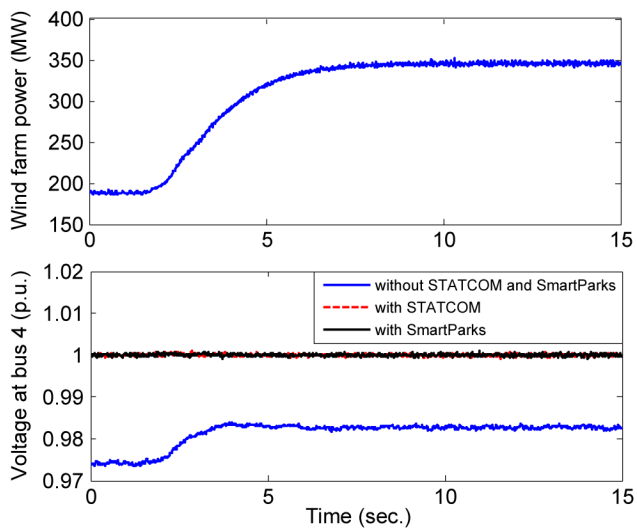

Fig. 15. Comparison of voltage control performance between STATCOM and SmartParks during wind power changes.

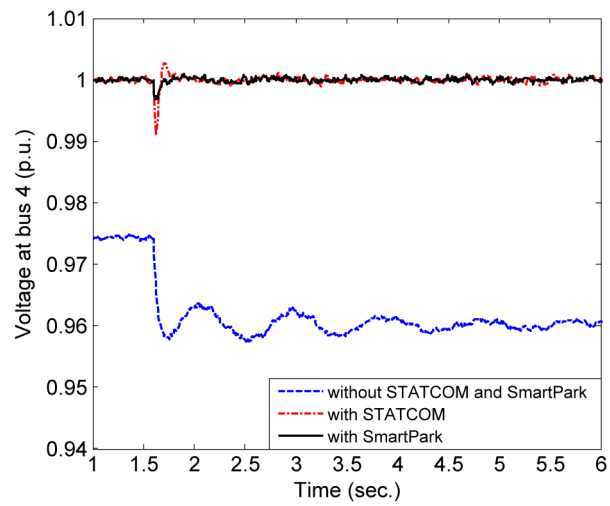

Fig. 16. Comparison of voltage control performance between STATCOM and SmartParks during line outage.

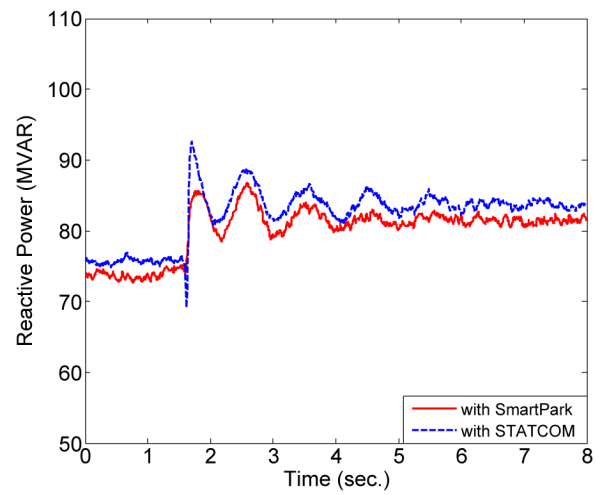

Fig. 17. Comparison of reactive power injection between STATCOM and SmartParks during line outage.

voltage at bus 4 also changes to 0.983 p.u., as shown in Fig. 15. However, with the STATCOM or the SmartParks in voltage control mode, at both of these operating points, the voltage at bus 4 can be maintained successfully at 1.0 p.u., as shown in Fig. 15.

Another contingency was studied by tripping one of the two parallel transmission lines connecting bus 4 and bus 3 in the test system. Fig. 16 compares the actual STATCOM and the SmartParks in terms of the voltage at bus 4 without any reactive power compensation. After the line outage, the voltage at bus 4 without any reactive compensation decreases to 0.96 p.u. However, with the reactive power support from the STATCOM or the SmartParks, the voltage can easily be maintained at 1.0 p.u. The voltage dip during the contingency is even lower with the SmartParks than with the STATCOM, as shown in Fig. 16. The reactive power injections for this contingency are compared in Fig. 17, which shows the characteristics shared by both methods.

Finally, a three-phase, 100 ms line-to-ground fault is applied at bus 4, and the bus 4 voltage and the reactive power injections are compared. It is observed in Fig. 18 that the SmartParks in voltage control mode behave as well as an actual STATCOM, even in the case of severe contingencies. The reactive power injection during the fault changes to almost 300 MVAR (Fig. 19), which remains within the total reactive power support capability of the 12 SmartParks (300 MVAR). From these results, it can be concluded that with a proper control strategy, the SmartParks can be utilized as virtual STATCOMs in the future, when the V2G transaction will become a reality.

B. Case Study 2

In order to study the performance of the coordinated reactive power support from the SmartParks, a 10-cycle, three-phase line to ground fault is applied at bus 6, where the wind farm is connected. Here, the crowbar operation starts the very moment the fault is applied and ends after 2 cycles from the instant of fault clearing. When there is no reactive power support from the GSC or from the SmartParks, the voltage at bus 6 takes almost 1.1 seconds to reach its prefault value, starting from the instant of fault application (Fig. 20). Also, the voltage waveform has a postfault, low-frequency oscillation in the absence of any kind of voltage control, whereas, with the SmartParks' coordinated

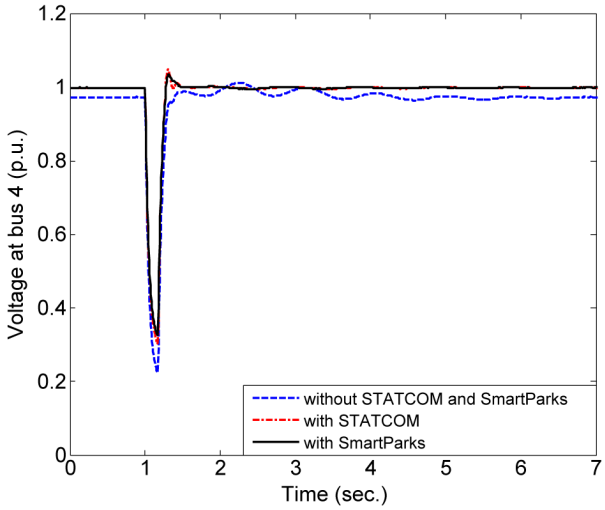

Fig. 18. Comparison of voltage control performance between STATCOM and SmartParks during a 100 ms three-phase fault at bus 4.

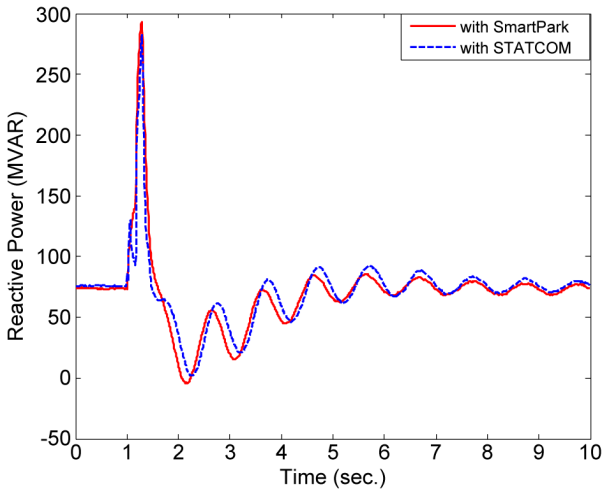

Fig. 19. Comparison of reactive power injection between STATCOM and SmartParks during a 100 ms three-phase fault at bus 4.

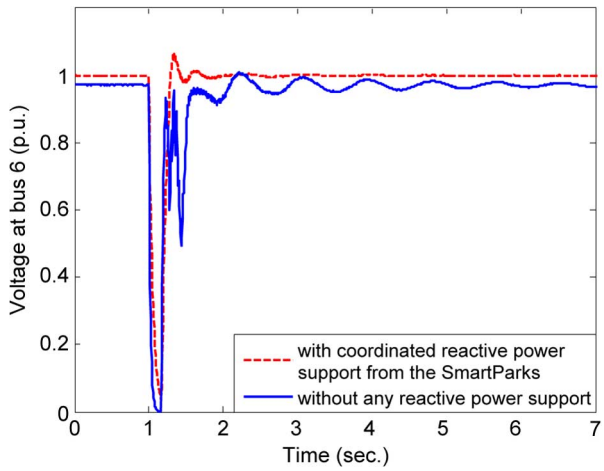

Fig. 20. Voltage at bus 6 with and without the coordinated reactive power supports from the SmartParks.

reactive power control, the voltage reaches 1.0 p.u. within 290 ms. After a small overshoot, it becomes perfectly stable.

Now, the performance of the coordinated control strategy is compared with the GSC being maintained at voltage control

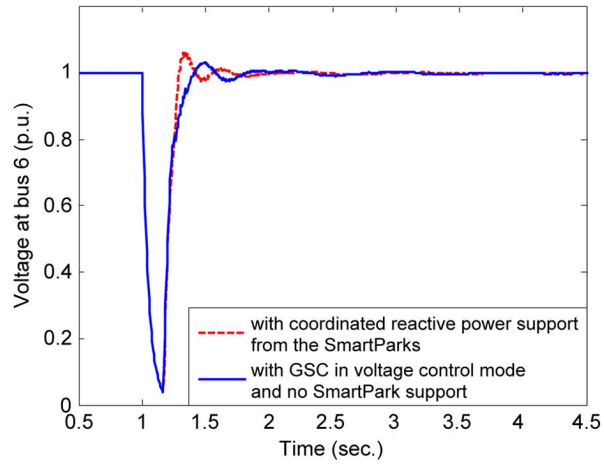

Fig. 21. Voltage at bus 6 with the coordinated reactive power supports from the SmartParks compared with GSC in voltage control mode.

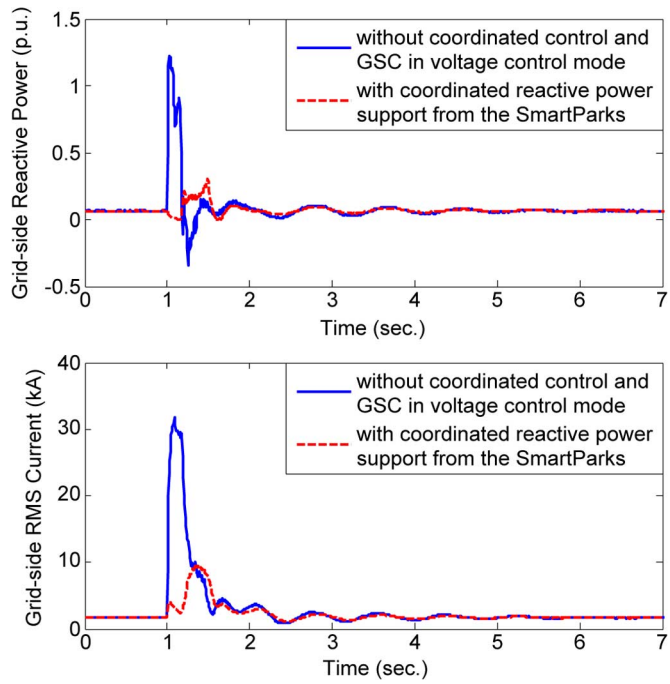

Fig. 22. Grid-side reactive power and rms current with the coordinated reactive power supports from the SmartParks compared with GSC in voltage control mode.

mode. But in this case, when the RSC is blocked, the GSC is not blocked, and it continues injecting reactive power during the fault. Fig. 21 shows that the voltage at bus 6 stabilizes quite nicely with this setup. The real problem, however, lies with the GSC current. If the GSC works in voltage control mode during the fault, the GSC current increases to almost 30 kA (Fig. 11), which is not permissible in practical situations. But, with the coordinated reactive power support from the SmartParks, i.e. with the GSC blocked during the fault and the voltage control action switched to the SmartParks, it is observed (Fig. 22) that the grid-side reactive power and the grid-side rms current both lie perfectly within their tolerable limits.

From these results, it can be concluded that the SmartParks can be utilized successfully as virtual STATCOMs for normal voltage regulation. Also, with a proper coordinated control strategy, they can improve the fault-ride-through performance

of the wind farms and facilitate their continuous operation during faults.

The integration of plug-in electric vehicles to power systems impacts the stability characteristics of the integrated systems. The necessity of wide area control (WAC) becomes more relevant during grid-to-vehicle (G2V) or vehicle-to-grid power transactions, that is, the charging and discharging cycles of the PEVs, respectively. The design of a WAC for providing damping to three generators in a 12-bus power system with PEVs was presented in a study by the authors in [25].

Furthermore, under a known range of SmartPark sizes, as well as a wide range of fluctuations in wind speed, and, correspondingly, wind power outputs, optimal tuning of the PI controllers is essential, as shown in a separate study reported in [26].

VI. Conclusions

A novel idea to exploit the reactive power capabilities of a large number of plug-in vehicles in SmartParks and utilizing the aggregation as a virtual STATCOM has been presented in this paper. First, a methodical analysis is carried out to obtain a realistic assessment of the reactive power capability of a commercially available hybrid vehicle battery. From there, an aggregated SmartPark model is developed on a real-time digital simulator platform, and 12 such SmartPark models are integrated into a 12-bus power system. The SmartParks' performance is compared with that of an actual STATCOM under various contingencies. Finally, a coordinated reactive power support strategy between the SmartParks and the grid-side converter of the wind farm is presented to improve the fault-ride-through capability of the wind farm while maintaining the continuity of service and without violating the grid-side reactive power and current limits.

References

[1] J. Tomić and W. Kempton, "Using fleets of electric drive vehicles for grid support," *J. Power Sources*, vol. 168, no. 2, pp. 459–468, Jun. 2007.

[2] W. Kempton and J. Tomić, "Vehicle-to-grid power fundamentals: Calculating capacity and net revenue," *J. Power Sources*, vol. 144, no. 1, pp. 268–279, Jun. 2005.

[3] C. Guille and G. Gross, "A conceptual framework for the vehicle-to-grid (V2G) implementation," *Energy Policy*, vol. 37, no. 11, pp. 4379–4390, Nov. 2009.

[4] W. Kempton and J. Tomić, "Vehicle-to-grid power implementation: From stabilizing the grid to supporting large-scale renewable energy," *J. Power Sources*, vol. 144, no. 1, pp. 280–294, Jun. 2005.

[5] A. Y. Saber and G. K. Venayagamoorthy, "Intelligent unit commitment with vehicle-to-grid—A cost-emission optimization," *J. Power Sources*, vol. 195, no. 3, pp. 898–911, Feb. 2010.

[6] C. Hutson, G. K. Venayagamoorthy, and K. Corzine, "Intelligent scheduling of hybrid and electric vehicle storage capacity in a parking lot for profit maximization in grid power transactions," in *Proc. IEEE Energy 2030*, Nov. 17–18, 2008, pp. 1–8.

[7] M. C. Kisacikoglu, B. Ozpineci, and L. M. Tolbert, "Examination of a PHEV bidirectional charger system for V2G reactive power compensation," in *Proc. 2010 25th Annu. IEEE Appl. Power Electron. Conf. Expo. (APEC)*, pp. 458–465.

[8] I. Cvetkovic *et al.*, "Future home uninterruptable renewable energy system with vehicle-to-grid technology," in *Proc. Energy Convers. Congr. Expo. (ECCE'09)*, San Jose, CA, Sep. 20–24, 2009, pp. 2675–2681.

[9] N. G. Hingorani and L. Gyugyi, *Understanding FACTS: Concepts and Technology of Flexible AC Transmission Systems*. New York: IEEE Press, 2000.

[10] R. K. Varma, V. Khadkikara, and R. Seethapathy, "Nighttime application of PV solar farm as STATCOM to regulate grid voltage," *IEEE Trans. Energy Convers.*, vol. 24, no. 4, pp. 983–985, 2009.

[11] W. Qiao, G. K. Venayagamoorthy, and R. G. Harley, "Real-time implementation of a STATCOM on a wind farm equipped with doubly fed induction generators," *IEEE Trans. Ind. Appl.*, vol. 45, no. 1, pp. 98–107, Jan./Feb. 2009.

[12] W. Qiao, R. G. Harley, and G. K. Venayagamoorthy, "Coordinated reactive power control of a large wind farm and a STATCOM using heuristic dynamic programming," *IEEE Trans. Energy Convers.*, vol. 24, no. 2, pp. 493–503, 2009.

[13] V. Akhmatov, "Analysis of dynamic behavior of electric power systems with large amount of wind power," Ph.D. dissertation, Tech. Univ. Denmark, Kgs. Lyngby, Denmark, Apr. 2003.

[14] P. C. Krause, O. Wasynczuk, and S. D. Sudhoff, *Analysis of Electric Machinery and Drive Systems*. New York: IEEE Press, 2002.

[15] P. Hippe, *Windup in Control*. Berlin, Germany: Springer, 2006.

[16] SAFT Hybrid Electric Military Vehicle Data Sheet [Online]. Available: http://www.saftbatteries.com/doc/Documents/defence/Cube769/HEMV%205-8%20Data%20Sheet.74ee69b4-34ed-49b5-a870-bd5f6160ab8d.pdf

[17] G. Kissel, "SAE J1772 update for IEEE Standard 1809 Guide," in *Proc. Electric-Sourced Transp. Infrastructure Meeting*, Feb. 18, 2010 [Online]. Available: http://grouper.ieee.org/groups/earthobservationsSCC/IEEE_SAE_J1772_Update_10_02_08_Gery_Kissel.pdf

[18] K. Morrow, D. Karner, and J. Francfort, "Plug-in hybrid electric vehicle charging infrastructure review," Final Rep., Battelle Energy Alliance, Contract 58517, Nov. 2008 [Online]. Available: http://avt.inel.gov/pdf/phev/phevInfrastructureReport08.pdf

[19] S. Jiang, U. D. Annakkage, and A. M. Gole, "A platform for validation of FACTS models," *IEEE Trans. Power Del.*, vol. 21, pp. 484–491, Jan. 2006.

[20] S. Jiang, U. D. Annakkage, and A. M. Gole, "A platform for validation of FACTS models," *IEEE Trans. Power Del.*, vol. 21, no. 1, pp. 484–491, Jan. 2005.

[21] R. Pena, J. C. Clare, and G. M. Asher, "Doubly fed induction generator using back-to-back PWM converters and its application to variable-speed wind-energy generation," *IET Proc. Electr. Power Appl.*, vol. 143, no. 3, pp. 231–241, May 1996.

[22] J. Lopez, P. Sanchis, X. Roboam, and L. Marroyo, "Dynamic behavior of the doubly fed induction generator during three phase voltage dips," *IEEE Trans. Energy Convers.*, vol. 22, no. 3, pp. 709–717, Sep. 2007.

[23] J. Morren and S. W. H. de Hann, "Ride through of wind turbines with doubly-fed induction generator during a voltage dip," *IEEE Trans. Energy Convers.*, vol. 20, no. 2, pp. 435–441, Jun. 2005.

[24] S. Mohagheghi, G. K. Venayagamoorthy, S. Rajagopalan, and R. G. Harley, "Hardware implementation of a mamdani fuzzy logic controller for a static compensator in a multimachine power system," *IEEE Trans. Ind. Appl.*, vol. 45, no. 4, pp. 1535–1544, Jul./Aug. 2009.

[25] P. Mitra and G. K. Venayagamoorthy, "Wide area control for improving stability of a power system with plug-in electric vehicles," *IET Proc. Gener., Transm., Distrib.*, vol. 4, no. 10, pp. 1151–1163, 2010.

[26] P. Chakravarty and G. K. Venayagamoorthy, "Development of optimal controllers for a DFIG based wind farm in a smart grid under variable wind speed conditions," in *Proc. Int. Elect. Mach. Drives Conf.*, May 15–18, 2011, pp. 733–738.

Pinaki Mitra (S'08–M'10) was born in 1974. He received the B.E. and M.E. degrees in electrical engineering from Jadavpur University, Kolkata, India, in 1997 and 1999, respectively, and the Ph.D. degree from the Real-Time Power and Intelligent Systems Laboratory, Electrical and Computer Engineering Department, Missouri University of Science and Technology, Rolla, in 2010.

Currently he is working as an Associate Scientist in the Grid Systems R&D division of ABB, Chennai, India. He has coauthored seven refereed international journal papers and twenty international conference papers. His research interests include real-time modeling and control of VSC based multiterminal HVDC system, wind integration, and vehicle-to-grid power transactions in smart grid.

Dr. Mitra is a member of IEEE Power and Energy Society. He is the recipient of IEEE IAS St. Louis Section Outstanding Young Engineer Award and IEEE CIS Walter Karplus Award in 2009.

Ganesh Kumar Venayagamoorthy (S'91–M'97–SM'02) received the Ph.D. degree in electrical engineering from the University of Natal, Durban, South Africa, in 2002.

He was a Visiting Researcher with ABB Corporate Research, Sweden, in 2007. He is a Professor of Electrical and Computer Engineering, and the Founder and Director of the Real-Time Power and Intelligent Systems (RTPIS) Laboratory at the Missouri University of Science and Technology (Missouri S&T), Rolla. He has published 2 edited books, 6 book chapters, and over 90 refereed journals papers and 290 refereed conference proceeding papers. His research interests are in the development and applications of advanced computational algorithms for real-world applications, including power systems stability and control, smart grid applications, sensor networks and signal processing.

Dr. Venayagamoorthy is a Fellow of the Institution of Engineering and Technology (IET), UK, and the South African Institute of Electrical Engineers. He is a recipient of several awards including a 2007 U.S. Office of Naval Research Young Investigator Program Award, a 2004 NSF CAREER Award, the 2010 Innovation Award from St. Louis Academy of Science, the 2010 IEEE Region 5 Outstanding Member Award, the 2006 IEEE Power and Energy Society Outstanding Young Engineer Award, a 2008, 2007, and 2005 Missouri S&T Faculty Excellence Award, and a 2009 Missouri S&T Faculty Research Award. He has been involved in the leadership and organization of many conferences including the Chair of the 2011 IEEE Symposium of Computational Intelligence Applications in Smart Grid (CIASG). He is currently the Chair of the IEEE PES Working Group on Intelligent Control Systems, the Chair of IEEE Computational Intelligence Society (CIS) Task Force on Smart Grid, and the Chair of the IEEE PES Intelligent Systems Subcommittee. He is currently an Associate Editor of the IEEE TRANSACTIONS OF EVOLUTIONARY COMPUTATION and an Editor of the IEEE TRANSACTIONS ON SMART GRID.

Keith A. Corzine (S'92–M'97–SM'06) received the B.S.E.E., M.S.E.E., and Ph.D. degrees from the University of Missouri, Rolla, in 1992, 1994, and 1997, respectively.

He taught at the University of Wisconsin, Milwaukee, from 1997 to 2004 and is now a Professor at Missouri University of Science & Technology, Rolla. His research interests include power electronics, motor drives, naval ship propulsion systems, and electric machinery. He has published nearly 40 refereed journal papers, over 60 refereed international conference papers, and holds 3 U.S. patents related to power conversion.

Dr. Corzine is currently the IAS Chapter chair and is on the Nomination and Appointments Committee of the IEEE St. Louis Section.